AFRRI SCIENTIFIC REPORT

THE RADIATION ENVIRONMENT ABOVE AN AIR-GROUND INTERFACE COVERED WITH ^{60}Co

ARMED FORCES RADIOBIOLOGY RESEARCH INSTITUTE
Defense Atomic Support Agency
Bethesda, Maryland

AFRRI SR68-1
January 1968

THE RADIATION ENVIRONMENT ABOVE AN AIR-GROUND INTERFACE COVERED WITH ^{60}Co

C. W. GARRETT

R. E. CARTER
Chairman
Physical Sciences Department

HUGH B. MITCHELL
Colonel, USAF, MC
Director

ARMED FORCES RADIOBIOLOGY RESEARCH INSTITUTE
Defense Atomic Support Agency
Bethesda, Maryland

ACKNOWLEDGMENT

Significant benefit was derived from discussions with R. L. French, C. Eisenhauer, and M. J. Berger. R. E. Carter made a substantial contribution by providing encouragement and advice during the course of the study and by organizing and editing the final version of this report, and C. H. Poppe's editorial contribution was invaluable.

TABLE OF CONTENTS

LIST OF TABLES

LIST OF FIGURES

FOREWORD
(Nontechnical summary)

In studies of fallout radiation environments and in the development of fallout shielding methodology, the exposure rate 3 feet above an infinite ground surface uniformly covered with ^{60}Co is used as a basic normalizing parameter. The quantity often used as a measure of the exposure rate at a point is the buildup factor; that is, the ratio of the total exposure rate to the exposure rate contributed by photons which have not undergone a collision prior to reaching the point. Comparison of buildup factors is advantageous, since absolute source strengths need not be known, and, since the uncollided component of the exposure rate can be accurately calculated for the infinite plane geometry, knowledge of the buildup factor permits easy calculation of the total exposure rate.

Several experimental measurements and several theoretical calculations of the buildup factor 3 feet above a ^{60}Co covered air-ground interface have been performed. The experimentally determined values range from 1.15 to 1.38, and the calculated values range from 1.15 to 1.23. To narrow this range of uncertainty, the study reported herein hypothesized factors that could contribute to the differences in the reported values, and consisted of a series of Monte Carlo calculations which were performed to confirm or refute these hypotheses.

The results of the analysis indicate that the Monte Carlo procedure and the method of moments agree, and a value $1.21 \pm .02$ may be assigned to the buildup factor 3 feet above an infinite air-ground interface uniformly contaminated with ^{60}Co. Since differential angle and energy distributions of the photon number flux density were developed as a portion of the study, they are also tabulated in this report.

ABSTRACT

A review has been made of experimental and theoretical determinations of the buildup factor 3 feet above an infinite air-ground interface uniformly covered with ^{60}Co. Experimental values of the buildup factor range from 1.15 to 1.38 and theoretically calculated values range from 1.15 to 1.23. A new series of Monte Carlo calculations is reported that tests various hypotheses which could account for this range of uncertainty. It is concluded that the substitution of compressed air or water for soil (required in the theoretical method of moments) is valid and that any intrinsic differences between the moments method and Monte Carlo techniques can account for no more than a 2 percent difference in the estimation of the buildup factor. A best value of $1.21 \pm .02$ may be assigned to the buildup factor 3 feet above an infinite air-ground interface contaminated with ^{60}Co. Angle and energy distributions of the photon number flux density for this geometry are also presented.

I. INTRODUCTION

There has been much interest in and effort devoted to solving the general problem of gamma ray transport through materials. The basic theoretical problem to solve is that of a point isotropic source in an infinite homogeneous medium. An equivalent problem of special practical interest is that of an infinite isotropic source plane imbedded in an infinite medium, or on an interface between two different media. The nuclear weapons fallout problem is a well-known example of the latter.

In fallout technology, the buildup factor at a point 3 feet above the ground produced by a distribution of ^{60}Co on the ground surface has been frequently referred to and used as a basic normalizing parameter.* Therefore, there are several measurements[2,9,19-21] and several calculations[4-6,10,11,17,22] of this quantity.

These data are summarized in Table I and the geometry is illustrated in Figure 1. For the experiments, the quoted uncertainties in the buildup factor are about ± 5 percent, and there are experimental conditions which make the geometry less than ideal. Therefore, complete agreement with calculations is not expected.

Some of the calculations were done with Monte Carlo procedures, and the others were done by the method of moments. The latter method can obtain results with errors as small as ± 1 percent, but it requires that the composition of the "air" and "soil" both be the same, with only a difference in densities. A recent moments method calculation[5] for ^{60}Co and an air-compressed air geometry has obtained a buildup factor of $1.21 \pm .01$.

* As this report was being edited, a related publication has appeared: E. T. Clarke, Gamma-Ray Scattering near an Air-Ground Interface. Nucl. Sci. Eng. 27:394-402, 1967.

Table 1. Summary of Reported Buildup Factors 3 Feet above a Uniformly Contaminated ^{60}Co Field

Investigator	Method	Buildup factor	Notes
Rexroad and Schmoke[2,20]	Experimental	1.25	Ionization chamber measurements 3 ft above a large array of ^{60}Co point sources; results extrapolated to infinite field
Schlomm et al.[21]	Experimental	1.15 (G-M Tube) 1.18 (Film Pack)	29 detectors were used to measure ground level upper hemisphere component at the apex of a quadrant of ^{60}Co point sources; results extrapolated to obtain total scattered exposure rate 3 ft above an infinite field
Plummer and Miller[19]	Experimental	1.15	Ionization chamber measurements 3 ft above an encapsulated ^{60}Co tube source laid on ground surface; results extrapolated to infinite field
Berger[4]	Moments	1.22	Point source in infinite water geometry; results integrated over source-detector distance to obtain buildup factor for plane source; function fitting used to reconstruct flux density
Spencer[22]	Moments	1.21	Infinite plane source in an infinite water medium used to calculate upper hemisphere contribution, assumed equal to lower hemisphere scattered contribution; function fitting used to reconstruct flux density
Hubbell[6]	Moments	1.23	Infinite plane source in an infinite water medium; polynomial expansion used to reconstruct flux density
National Bureau of Standards[3]	Moments	1.21	Infinite plane source in an infinite air medium; polynomial expansion used to reconstruct flux density
Berger[4]	Monte Carlo	1.22	Point source in infinite water medium, results integrated over source-detector distance; 10,000 histories
Marcum[17]	Monte Carlo	1.16	Point source in air-compressed air geometry, results integrated over source-detector distance to obtain buildup factor, point sources were located 2 in. above interface, 12,750 histories
Trubey[10]	Monte Carlo	1.15	Distributed point sources in air-ground geometry; DOT procedure used; 2,300 histories
Trubey[11]	Monte Carlo	1.18	As above except that the COHORT procedure was used; 7000 histories

On the other hand, the Monte Carlo procedure can accurately simulate actual air and actual soil but, because of the long computer times required, the smallest error obtained in the buildup factor is about ±3 percent.

In addition to the random errors in the calculations, there are certain assumptions which could lead to consistently different answers by the two methods, and not all of the effects of these assumptions have been systematically explored. For

example, in the moments method, water (with appropriate density adjustments) has been substituted for air. Also, in order to conserve computing time, in both Monte Carlo and moments method calculations, photons have been ignored once they have scattered down to some cutoff energy, such as 0.06 or 0.1 MeV. On the basis of data then available, Garrett[12] questioned both of these hypotheses. Subsequent results of Marshall and Wells[18] and Alberg et al.[1] indicated that water can be validly substituted for air, but that photons in the energy interval between 0.06 - 0.10 MeV cannot be ignored. Additional calculations discussed in this report confirm these conclusions, but they also suggest a reason for the Monte Carlo values being consistently lower than those of the moments method, as observed in the results of French.[10]

Another possible but not very probable explanation for the difference between Monte Carlo and moments method results is that an inherent difference in the two

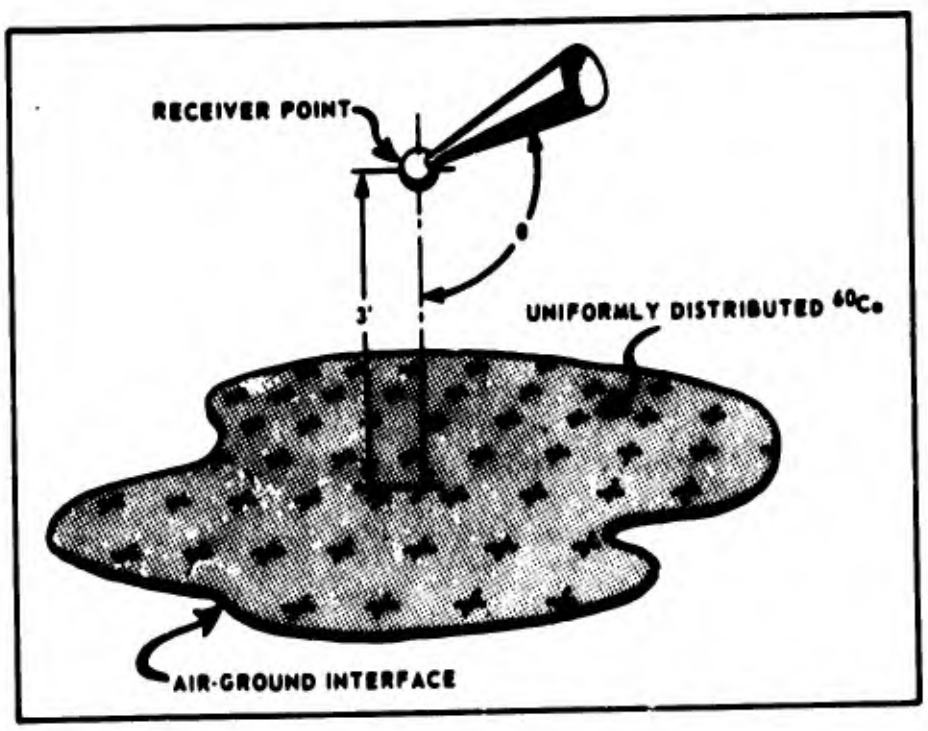

Figure 1. Air-ground geometry

mathematical procedures exists such that Monte Carlo estimates of the flux densities converge toward a different, lower value than do estimates generated by the method of moments. Such an effect might result, for example, from the manner chosen to reconstruct the flux densities[13] using a finite set of calculated moments and/or from the properties of the pseudorandom number generators used in Monte Carlo procedures.

French computed the angle and energy distributions of the photon flux density at a receiver point 3 feet above an air-ground interface for each of 10 monoenergetic sources uniformly distributed on the interface. The contribution from unscattered photons was calculated by an analytic procedure, and the scattered component was computed with the LO5 Monte Carlo program.[7] By appropriate weighting of the results for each source, the photon flux density distribution for weapons fallout of a given age can be obtained.

French also computed the kerma rate* in tissue due to each of these monoenergetic sources from which tissue dose buildup factors can be obtained. One of the source energies was 1.25 MeV, representative of ^{60}Co, from which the exposure buildup factor of 1.15 was derived.

In French's calculation, the objective was primarily to construct a fallout simulation, and not to determine accurately the ^{60}Co buildup factor. Therefore, he followed only 2300 histories at each source energy and a history was terminated either after 15 collisions, or when the photon energy fell below 0.04 MeV, whichever occurred first.

* French refers to the quantity as "absorbed dose rate".

Because of the low value obtained for the ^{60}Co buildup factor from these results, some question arose about the possibility of a systematic difference between the results to be expected from the Monte Carlo and the moments methods. Therefore, new sets of computations were run by the Monte Carlo procedure, with more conservative limits for discarding scattered photons, and with a large enough set of histories so that statistical variations allow valid conclusions. The remainder of this report discusses these calculations.

II. EXTENDED AIR-GROUND CALCULATIONS

Kalos[15] noted that the statistical estimation technique in the LO5 Monte Carlo procedure tends to underestimate the exposure rate unless a sufficient number of histories is followed. Also Garrett[12] and Marshall and Wells[18] reported that in low-Z materials, low-energy (< 0.10 MeV) photons might contribute significantly to the kerma rate. To determine if one or both of these effects caused the apparently low buildup factor in the French computations, his calculations of the scattered component of the flux density above an infinite ^{60}Co plane were extended by increasing the number of histories followed and by lowering the photon low-energy cutoff point.

In the extended calculations, the geometry, source distribution, cross sections, and LO5 Monte Carlo procedure were identical to those used by French.[10] However, photon histories were not terminated until either 45 collisions occurred or the photon's energy dropped below 0.02 MeV. Under these criteria, 98 percent of the 19,320 histories followed were terminated by the low-energy cutoff. The 10-degree wide receiver polar angle bins of French were retained, as were his eight receiver energy

bins. However, two additional energy bins were added in the new calculations to cover the interval from 0.02 to 0.04 MeV.

The results of the extended calculations are shown in Table II, which gives the total scattered photon flux density in each angle-energy bin; appropriate differential distributions can be obtained by dividing the tabulated value by the respective bin width. The flux densities summed over energy intervals are given in the rightmost column, and those summed over angle intervals are listed in the last row. All data are normalized to one 1.25 MeV source photon emitted isotropically per unit source area per second. The data in Table II have not been smoothed in any way.

Table II. Angle and Energy Distribution of the Scattered Photon Number Flux Density 3 Feet above an Infinite, Uniformly Contaminated Ground Surface Emitting One 1.25 MeV Photon per Unit Area per Second

Polar angle bins (degrees)*	Receiver energy bins (MeV)*										
	0.03*	0.04	0.06	0.10	0.18	0.30	0.50	0.75	1.00	1.25	Sum
10	9.528(-9)†	6.920(-6)	1.609(-4)	1.041(-3)	1.252(-3)	1.904(-3)	7.334(-3)	0.	0.	0.	5.098(-3)
20	1.842(-8)	5.643(-6)	3.074(-4)	2.246(-3)	3.796(-3)	7.751(-3)	2.338(-3)	2.337(-4)	0.	0.	1.668(-2)
30	2.433(-8)	1.707(-5)	5.733(-4)	4.888(-3)	8.856(-3)	1.188(-2)	4.110(-3)	5.723(-4)	0.	0.	3.090(-2)
40	7.583(-8)	2.346(-5)	1.065(-3)	4.172(-3)	1.208(-2)	1.411(-2)	8.024(-3)	1.705(-3)	0.	0.	4.118(-2)
50	2.148(-8)	1.168(-5)	1.342(-3)	9.811(-3)	8.940(-3)	1.532(-2)	8.526(-3)	2.479(-3)	1.879(-3)	0.	4.831(-2)
60	6.171(-9)	5.986(-5)	2.332(-3)	9.244(-3)	1.381(-2)	1.597(-2)	1.047(-2)	6.763(-3)	1.524(-3)	0.	6.018(-2)
70	5.967(-8)	2.568(-5)	1.091(-3)	1.959(-2)	2.001(-2)	1.922(-2)	1.307(-2)	9.472(-3)	1.006(-2)	7.726(-4)	9.331(-2)
80	3.728(-6)	1.109(-5)	7.657(-3)	1.202(-2)	1.747(-2)	2.814(-2)	1.749(-2)	1.584(-2)	1.413(-2)	1.262(-2)	1.254(-1)
90	2.055(-4)	1.922(-4)	1.569(-2)	1.210(-2)	3.422(-2)	2.964(-2)	1.840(-2)	2.234(-2)	2.331(-2)	5.916(-2)	2.153(-1)
100	1.715(-4)	9.433(-4)	9.255(-3)	2.968(-2)	3.881(-2)	2.777(-2)	2.267(-2)	1.447(-2)	2.217(-2)	9.519(-2)	2.611(-1)
110	2.255(-5)	1.900(-3)	1.178(-2)	2.176(-2)	3.948(-2)	3.060(-2)	1.384(-2)	1.522(-2)	7.066(-3)	1.326(-3)	1.430(-1)
120	8.382(-5)	1.468(-3)	1.062(-2)	2.770(-2)	2.269(-2)	2.748(-2)	2.159(-2)	5.759(-3)	2.989(-3)	0.	1.204(-1)
130	8.132(-5)	6.061(-3)	1.045(-2)	1.158(-2)	2.149(-2)	2.502(-2)	7.280(-3)	1.258(-2)	0.	0.	9.454(-2)
140	2.738(-4)	1.498(-3)	7.519(-3)	1.014(-2)	1.393(-2)	2.027(-2)	6.917(-3)	2.851(-4)	0.	0.	6.083(-2)
150	5.630(-4)	8.066(-4)	6.212(-3)	1.286(-2)	2.063(-2)	8.030(-3)	3.111(-3)	0.	0.	0.	5.222(-2)
160	4.974(-5)	1.757(-3)	2.142(-3)	1.455(-2)	1.600(-2)	6.399(-3)	5.517(-3)	0.	0.	0.	4.642(-2)
170	1.336(-5)	5.290(-4)	2.591(-3)	4.533(-3)	4.330(-3)	2.445(-3)	2.892(-2)	0.	0.	0.	4.336(-2)
180	2.832(-6)	1.804(-4)	2.352(-3)	2.129(-3)	1.267(-3)	2.185(-3)	0.	0.	0.	0.	8.117(-3)
Sum	1.471(-3)	1.550(-2)	9.315(-2)	2.100(-1)	2.991(-1)	2.941(-1)	1.930(-1)	1.077(-1)	8.313(-2)	1.691(-1)	
										Total	1.466

* Each bin heading gives the upper limit of that bin

* Lower bound of 0.03 column is 0.02 MeV

† Read 9.528(-9) as 9.528×10^{-9}

The kerma rates in air were computed from the number flux densities of Table II, using conversion factors from Henderson[14] for the midpoints of the energy intervals. Table III shows the results of this computation. Values obtained from a more recent calculation of French[11] which used the COHORT Monte Carlo procedure[8] are shown for comparison purposes in the fifth column. Kerma rates derived from the extended calculation are shown in the sixth column. At the bottom of Table III, the value for the uncollided 1.25 MeV flux density, computed analytically by French (Reference 10, Table 1), and its kerma rate are given. Using these results, the

Table III. Scattered Kerma Rates* in Air 3 Feet above an Infinite ^{60}Co Contaminated Plane

Energy interval (MeV)	Fluence-to-kerma factor (ergs cm^2 g^{-1})	French† flux density (cm^{-2} sec^{-1})	French† kerma rate (ergs g^{-1} sec^{-1})	French COHORT kerma rate‡ (ergs g^{-1} sec^{-1})	Extended calculation kerma rate (ergs g^{-1} sec^{-1})
.02 - .03	1.06(-8)§	-	-	-	1.56(-11)
.03 - .04	5.28(-9)	-	-	-	8.18(-11)
.04 - .06	3.06(-9)	4.45(-2)	1.36(-10)	2.70(-10)	2.85(-10)
.06 - .10	3.06(-9)	1.73(-1)	5.31(-10)	6.74(-10)	6.42(-10)
.10 - .18	5.56(-9)	1.91(-1)	1.06(-9)	1.50(-9)	1.66(-9)
.18 - .30	1.08(-8)	2.40(-1)	2.60(-9)	3.76(-9)	3.19(-9)
.30 - .50	1.89(-8)	1.25(-1)	2.37(-9)	2.45(-9)	3.65(-9)
.50 - .75	2.92(-8)	8.01(-2)	2.33(-9)	3.42(-9)	3.14(-9)
.75 - 1.00	3.97(-8)	6.60(-2)	2.64(-9)	4.35(-9)	3.30(-9)
1.00 - 1.25	5.00(-8)	1.31(-1)	6.67(-9)	3.72(-9)	8.46(-9)
Total		1.05(-0)	1.83(-8)	2.01(-8)	2.44(-8)
Uncollided flux density** = 2.217 photons cm^{-2} sec^{-1}					
Uncollided kerma rate = 1.184 x 10^{-7} ergs g^{-1} sec^{-1}					

* Normalized to one 1.25 MeV photon cm^{-2} sec^{-1} emitted isotropically
† Reference 10, Table 2
‡ Derived from reference 11
§ Read 1.06(-8) as 1.06 x 10^{-8}
** Reference 10, Table 1

buildup factor for the extended calculation of the air-ground geometry is found to be

$$1 + \frac{2.44 \times 10^{-8}}{1.184 \times 10^{-7}} = 1.21$$

as compared with French's original value of 1.15.

To evaluate the accuracy of the result, the standard deviations in these Monte Carlo calculations should be obtained. The LO5 procedure computes the deviation of sample values (treating each history as a sample) about the total collided number flux density. However, since the estimator used in the statistical estimation process has an infinite variance,[15*] the deviation computed by the LO5 program cannot be interpreted as the standard deviation about the expected total flux density. The best that may be done is to make a judgment of the possible error based upon experience with the LO5 program.

For the extended calculation, the LO5-computed deviation was 7.5 percent of the total collided flux density. When deviations of this size have been encountered during applications of LO5 to problems whose solutions are known with high precision (i.e., calculation of buildup factors in an infinite water, isotropic ^{60}Co point source geometry), computational errors of less than 10 percent were usually observed in flux density estimates. Therefore, it is assumed that no greater than a 10 percent error actually occurred in the extended air-ground calculations. Making the further assumption that the percent error in the kerma rate from collided photons is equal to that of the computed total collided flux density, the value for the buildup factor becomes $1.21 \pm .02$. This value is consistent with the moments method results and lies in the midrange of the reported experimental data.

* See also Appendix A

An examination of Table III shows that an increase in scattered flux density occurred in each energy interval so that the energy spectrum of the extended calculations is very similar to that of the French data. Approximately 4 percent of the kerma was delivered by photons below 0.1 MeV; however, less than 0.5 percent was contributed by photons below 0.04 MeV. Therefore, the low value of French's original buildup factor cannot be accounted for by his choice of low-energy and maximum collision cutoffs but, rather, by the effect described by Kalos. The 2300 histories of the original calculation resulted in an underestimate of the number flux density but the 19,320 histories followed in the extended calculations appear to have been sufficient to overcome this difficulty.

III. AIR-COMPRESSED AIR MONTE CARLO CALCULATIONS

High accuracy is obtainable with the moments method, so it is desirable to utilize this method to obtain a precise value for the buildup factor. However, moments method calculations are limited to the use of one scattering material to represent both air and ground, and investigators have chosen either air or water, scaling densities as required, to represent the air above and soil below the interface.

The validity of using water to represent air has been well established. The use of compressed air to represent soil was recently examined by Beck and Bennett[3] who found that the scattered kerma rate 1 meter above an air-ground interface contaminated with ^{137}Cs was 7 percent lower than that above an air-compressed air interface. (The difference between the buildup factors of the two cases would be 1 percent.) Beck and Bennett utilized a polynomial expansion technique to solve the transport equation for the two-medium geometry.

At the suggestion of C. Eisenhauer of the National Bureau of Standards (NBS), a set of Monte Carlo computations has been performed using the LO5 Monte Carlo procedure to further examine the effect of the substitution of compressed air for soil and to provide a direct comparison between a moments method and a Monte Carlo solution of the interface problem. A ^{60}Co source was used on the interface for this Monte Carlo study.

The geometry employed was identical to that of the extended air-ground calculations except that to provide a direct comparison with the National Bureau of Standards moments calculation,[5] compressed air was used to represent soil. This compressed air region consisted of 78.47 percent nitrogen, 21.06 percent oxygen and 0.47 percent argon (atomic fractions); the air density was adjusted such that the electron density was 3.5×10^{23} electrons cm^{-3}. This is identical to the electron density of the soil used both in French's original calculations and in our extended air-ground calculations. The aboveground air density was chosen to be 1.205×10^{-3} g cm^{-3}, identical to that of the NBS calculations.

The decision to equate the electron density of the compressed air with that of the soil was arbitrary; equating atomic concentrations or mass densities could also have been done. However, the application of a theorem (attributed to U. Fano) shows that the choice should not affect the results of the computation. The theorem states that for distance measured in terms of mean free paths, the exposure rate at a given distance above an isotropic infinite plane source in an infinite medium is independent of density variations in the direction normal to the source plane.

The cross-section library for air used in the LO5 procedure was that used in the extended calculations and was also identical to that used by NBS in their moments calculation. At 1.25 MeV, the total mass attenuation coefficient was 0.0568 $cm^2\ g^{-1}$.

A total of 57,500 photon histories were followed, 2500 from each of 23 isotropic point sources distributed on the air-compressed air interface. The placement of these point sources was identical to that used by French[10] and to that used in the extended air-ground calculations. Histories were terminated when a photon's energy dropped below 0.02 MeV or after 23 collisions had occurred. With these limits, over 90 percent of the photons reached 0.04 MeV and 80 percent reached 0.03 MeV before being terminated by the maximum collision criterion.

The calculation was divided into five 11,500-history segments to permit reasonable computing times, and the results of these separate computations illustrate the difficulties of using an unbiased Monte Carlo statistical estimation procedure for this type of problem. The five calculations were identical in all respects except that different random numbers were chosen to initiate each calculation. Table IV summarizes the results of each 11,500-history case. The total scattered number flux density, the LO5 computed percent deviation in the flux density, and the total kerma rate are listed for the five cases. The kerma rate was calculated in a manner identical to that used in the extended air-ground calculations. It is clear from the data in Table IV that 11,500 histories are not sufficient to guarantee reasonable accuracy and, further, that the fourth case, D, merits additional scrutiny.

The reason for the results of case D is evident when the differential angle and energy distributions of that case are compared with the equivalent distributions of the

Table IV. Results of Five 11,500-History Cases

Case	Total scattered flux density (cm^{-2} sec^{-1})	Percent deviation about total scattered flux density	Total scattered kerma rate (ergs g^{-1} sec^{-1})
A	1.89	25	2.76×10^{-8}
B	1.99	16	3.10×10^{-8}
C	1.60	15	2.03×10^{-8}
D	3.51	59	3.10×10^{-8}
E	1.35	7	2.00×10^{-8}
D*	1.38	16	2.03×10^{-8}

* Adjusted values for case D; see text

other four cases. These distributions for case D are shown in Table V in a format identical to that of Table II. Table VI lists the distributions obtained by averaging the data from cases A, B, C and E, and Table VII lists the distributions obtained by averaging all five cases. Examination of the tables shows that above 0.06 MeV the distributions of case D look reasonable and show fluctuations of the same order of magnitude as those found in the other four cases.

However, in the three lowest energy intervals of case D, and (coincidentally) in the same angle interval of 30°-40°, the effects of a severe close-in collision problem are observed. In these three bins, close-in collisions accounted for such high flux density estimates that the contents of the three bins contributed 60 percent of the total scattered flux density and 35 percent of the equivalent total kerma rate. Even when averaged with the other four cases (Table VII), the fluctuations of case D are not obscured. In this situation, the effects of the close-in collisions in case D cannot be ignored, and either the case must be rejected, or adjustments must be made.

Table V. Angle and Energy Distribution of the Scattered Photon Number Flux Density 3 Feet above an Infinite, Uniformly Contaminated Condensed Air Surface Emitting One 1.25 MeV Photon per Unit Area per Second. Case D -- 11,500 Histories

Polar angle bins (degrees)*	Receiver energy bins (MeV)*										
	0.03*	0.04	0.06	0.10	0.18	0.30	0.50	0.75	1.00	1.25	Sum
10	5.707(-7)†	5.772(-5)	2.549(-4)	1.238(-3)	1.700(-3)	1.722(-3)	3.276(-3)	3.779(-6)	0.	0.	8.255(-3)
20	1.801(-5)	2.870(-4)	1.829(-3)	2.870(-3)	4.351(-3)	7.880(-3)	2.831(-3)	7.588(-6)	0.	0.	2.007(-2)
30	1.682(-5)	3.735(-4)	1.914(-3)	4.973(-3)	5.680(-3)	9.334(-3)	5.532(-3)	5.663(-5)	0.	0.	2.788(-2)
40	1.830(-1)	1.333	6.099(-1)	5.213(-3)	8.714(-3)	1.231(-2)	6.476(-3)	1.905(-3)	0.	0.	2.161
50	2.211(-5)	3.596(-4)	5.273(-2)	5.990(-3)	9.583(-3)	1.451(-2)	8.155(-3)	7.649(-3)	0.	0.	9.900(-2)
60	9.983(-6)	4.713(-4)	3.643(-3)	6.896(-3)	9.791(-3)	1.717(-2)	9.929(-3)	8.977(-3)	1.476(-3)	0.	5.836(-2)
70	2.126(-5)	7.872(-4)	3.846(-3)	8.829(-3)	2.396(-2)	2.305(-2)	1.209(-2)	1.233(-2)	1.854(-3)	0.	8.977(-2)
80	7.431(-5)	8.537(-4)	1.402(-2)	1.536(-2)	1.842(-2)	2.054(-2)	1.522(-2)	1.586(-2)	1.799(-2)	1.833(-2)	1.647(-1)
90	9.046(-5)	1.894(-3)	2.243(-2)	9.459(-3)	2.172(-2)	2.419(-2)	2.218(-2)	2.003(-2)	2.331(-2)	3.754(-2)	1.828(-1)
100	4.246(-4)	2.692(-3)	1.589(-2)	2.075(-2)	3.362(-2)	2.823(-2)	3.432(-2)	1.821(-2)	1.908(-2)	2.566(-2)	1.988(-1)
110	1.790(-4)	4.089(-3)	1.173(-2)	2.743(-2)	2.[illegible](-2)	1.476(-2)	1.474(-2)	1.577(-2)	5.346(-3)	7.159(-4)	1.220(-1)
120	1.857(-4)	2.653(-3)	2.365(-2)	1.854(-2)	2.674(-2)	2.191(-2)	9.902(-3)	7.349(-3)	0.	0.	1.109(-1)
130	1.433(-4)	1.703(-3)	7.968(-3)	1.609(-2)	2.652(-2)	2.283(-2)	6.319(-3)	4.366(-5)	0.	0.	8.162(-2)
140	6.377(-5)	1.101(-3)	2.047(-2)	3.817(-2)	1.112(-2)	1.087(-2)	2.703(-3)	1.508(-5)	0.	0.	8.451(-2)
150	1.261(-4)	1.478(-3)	5.972(-3)	1.036(-2)	1.959(-2)	9.461(-3)	2.861(-3)	1.343(-5)	0.	0.	4.986(-2)
160	6.255(-5)	8.430(-4)	4.528(-3)	7.116(-3)	6.134(-3)	6.563(-3)	6.607(-4)	8.339(-6)	0.	0.	2.592(-2)
170	1.993(-5)	1.518(-3)	4.542(-3)	3.351(-3)	7.757(-3)	3.864(-3)	3.631(-4)	3.717(-6)	0.	0.	2.142(-2)
180	1.496(-6)	4.597(-4)	4.543(-3)	7.465(-4)	8.696(-4)	5.022(-4)	0.	2.922(-7)	0.	0.	7.123(-3)
Sum	1.845(-1)	1.355	8.098(-1)	2.034(-1)	2.585(-1)	2.497(-1)	1.576(-1)	1.112(-1)	7.203(-2)	1.122(-1)	3.514

* Each bin heading gives the upper limit of that bin
* Lower bound of 0.03 column is 0.02 MeV
† Read 5.707(-7) as 5.707×10^{-7}

Table VI. Angle and Energy Distribution of the Scattered Photon Number Flux Density 3 Feet above an Infinite, Uniformly Contaminated Condensed Air Surface Emitting One 1.25 MeV Photon per Unit Area per Second. Cases A, B, C, E -- 46,000 Histories

Polar angle bins (degrees)*	Receiver energy bins (MeV)*										
	0.03*	0.04	0.06	0.10	0.18	0.30	0.50	0.75	1.00	1.25	Sum
10	5.928(-6)†	7.744(-5)	4.119(-4)	8.810(-4)	9.607(-4)	1.551(-3)	9.394(-4)	3.115(-5)	0.	2.316(-5)	4.882(-3)
20	1.063(-5)	2.116(-4)	1.259(-3)	2.506(-3)	4.050(-3)	5.174(-3)	2.670(-3)	6.615(-6)	0.	0.	1.589(-2)
30	2.852(-5)	4.375(-4)	2.140(-3)	4.502(-3)	6.802(-3)	8.553(-3)	4.535(-3)	1.951(-4)	0.	8.910(-5)	2.734(-2)
40	3.649(-5)	5.047(-4)	1.617(-2)	1.892(-2)	7.353(-3)	1.133(-2)	5.856(-3)	1.421(-3)	8.632(-5)	0.	6.168(-2)
50	5.038(-4)	5.968(-4)	2.958(-3)	6.527(-3)	9.530(-3)	1.400(-2)	7.644(-3)	3.709(-3)	1.235(-4)	0.	1.560(-2)
60	7.534(-5)	6.637(-4)	3.886(-3)	7.942(-3)	1.396(-2)	1.689(-2)	1.063(-2)	6.850(-3)	2.217(-3)	0.	6.311(-2)
70	6.788(-5)	4.527(-4)	5.102(-3)	9.205(-3)	1.491(-2)	1.820(-2)	1.571(-2)	1.121(-2)	1.355(-2)	2.123(-3)	9.084(-2)
80	5.830(-5)	9.844(-4)	1.062(-2)	3.384(-2)	2.644(-2)	1.189(-1)	1.845(-2)	1.893(-2)	1.583(-2)	8.167(-3)	2.523(-1)
90	1.991(-4)	2.089(-3)	1.208(-2)	1.953(-2)	2.720(-2)	3.312(-2)	2.230(-2)	3.262(-2)	2.998(-2)	4.173(-2)	2.209(-1)
100	1.727(-4)	7.807(-3)	1.143(-2)	4.100(-2)	7.953(-2)	3.463(-2)	1.891(-2)	2.037(-2)	1.505(-2)	5.820(-2)	4.071(-1)
110	2.925(-4)	3.145(-3)	1.318(-2)	3.222(-2)	2.526(-2)	2.426(-2)	1.327(-2)	1.068(-2)	8.243(-3)	9.957(-3)	1.105(-1)
120	2.734(-3)	3.726(-3)	1.113(-2)	5.415(-2)	2.380(-2)	2.494(-2)	1.615(-2)	6.823(-3)	5.657(-3)	0.	1.491(-1)
130	2.439(-4)	4.245(-3)	1.280(-2)	1.961(-2)	1.896(-2)	1.707(-2)	1.280(-2)	7.475(-3)	0.	0.	9.320(-2)
140	2.340(-4)	2.498(-3)	9.662(-3)	1.581(-2)	2.498(-2)	9.885(-3)	2.079(-2)	2.422(-5)	0.	0.	8.389(-2)
150	1.129(-4)	2.834(-3)	6.344(-3)	3.678(-2)	1.181(-2)	8.629(-3)	1.076(-3)	1.201(-5)	0.	0.	7.058(-2)
160	6.500(-5)	1.681(-3)	8.958(-3)	9.463(-3)	7.411(-3)	1.221(-2)	5.251(-5)	1.219(-5)	0.	0.	4.506(-2)
170	4.865(-5)	4.799(-4)	3.798(-3)	3.616(-3)	5.120(-3)	8.966(-3)	1.091(-3)	6.803(-6)	0.	0.	2.313(-2)
180	2.158(-5)	8.635(-5)	8.211(-4)	1.689(-3)	1.441(-3)	1.591(-3)	6.119(-4)	3.596(-6)	0.	0.	1.126(-2)
Sum	4.911(-3)	3.252(-2)	1.330(-1)	3.202(-1)	3.125(-1)	3.699(-1)	1.817(-1)	1.204(-1)	1.107(-1)	1.206(-1)	1.707

* Each bin heading gives the upper limit of that bin
* Lower bound of 0.03 column is 0.02 MeV
† Read 5.928(-6) as 5.928×10^{-6}

Table VII. Angle and Energy Distribution of the Scattered Photon Number Flux Density 3 Feet above an Infinite, Uniformly Contaminated Condensed Air Surface Emitting One 1.25 MeV Photon per Unit Area per Second. Cases A-E -- 57,500 Histories

Polar angle bins (degrees)*	Receiver energy bins (MeV)*										
	0.03*	0.04	0.06	0.10	0.18	0.30	0.50	0.75	1.00	1.25	Sum
10	4.857(-6)†	7.450(-5)	3.805(-4)	9.524(-4)	1.109(-3)	1.585(-3)	1.407(-3)	2.608(-5)	0.	1.853(-5)	5.557(-3)
20	1.210(-5)	2.267(-4)	1.373(-3)	2.579(-3)	4.110(-3)	5.715(-3)	2.702(-3)	6.810(-6)	0.	0.	1.673(-2)
30	2.618(-5)	1.247(-4)	2.095(-3)	4.644(-3)	6.577(-3)	8.710(-3)	4.735(-3)	1.674(-4)	0.	7.128(-5)	2.745(-2)
40	4.663(-5)	2.670(-4)	1.349(-3)	1.618(-2)	7.625(-3)	1.154(-2)	5.980(-3)	1.518(-3)	6.906(-5)	0.	4.815(-2)
50	4.075(-4)	5.494(-4)	1.291(-2)	6.420(-3)	9.541(-3)	1.410(-2)	7.747(-3)	4.497(-3)	9.884(-5)	0.	5.628(-2)
60	6.227(-5)	6.252(-4)	3.837(-3)	7.733(-3)	1.313(-2)	1.694(-2)	1.049(-2)	7.276(-3)	2.089(-3)	0.	6.216(-2)
70	5.856(-5)	5.196(-4)	4.851(-3)	9.130(-3)	1.672(-2)	1.917(-2)	1.499(-2)	1.141(-2)	1.181(-2)	1.939(-3)	9.063(-2)
80	6.150(-5)	9.582(-4)	1.130(-2)	3.015(-2)	2.384(-2)	9.925(-2)	1.781(-2)	1.891(-2)	1.627(-2)	1.620(-2)	2.347(-1)
90	1.773(-4)	2.050(-3)	1.415(-2)	1.752(-2)	2.610(-2)	3.134(-2)	2.228(-2)	3.010(-2)	2.865(-2)	4.089(-2)	2.133(-1)
100	2.231(-4)	6.784(-3)	1.230(-2)	3.695(-2)	7.035(-2)	3.335(-2)	2.202(-2)	1.994(-2)	3.185(-2)	5.169(-2)	2.855(-1)
110	2.698(-4)	1.334(-2)	1.289(-2)	3.127(-2)	2.566(-2)	2.206(-2)	1.356(-2)	1.170(-2)	7.664(-3)	8.109(-3)	1.368(-1)
120	2.224(-3)	3.512(-3)	1.388(-2)	4.703(-2)	2.439(-2)	2.433(-2)	1.490(-2)	6.928(-3)	4.526(-3)	0.	1.417(-1)
130	2.237(-4)	3.736(-3)	1.183(-2)	1.890(-2)	2.047(-2)	1.822(-2)	1.151(-2)	5.989(-3)	0.	0.	9.089(-2)
140	1.999(-4)	2.218(-3)	1.182(-2)	2.028(-2)	2.221(-2)	1.008(-2)	1.717(-2)	2.239(-5)	0.	0.	8.401(-2)
150	1.155(-4)	2.563(-3)	6.270(-3)	3.149(-2)	1.336(-2)	8.788(-3)	3.833(-3)	1.229(-5)	0.	0.	6.644(-2)
160	6.451(-5)	1.513(-3)	8.072(-3)	8.994(-3)	7.161(-3)	1.108(-2)	4.333(-3)	1.137(-5)	0.	0.	4.123(-2)
170	4.291(-5)	6.875(-4)	3.947(-3)	3.563(-3)	5.647(-3)	7.946(-3)	9.457(-4)	6.186(-6)	0.	0.	2.278(-2)
180	1.756(-5)	1.610(-4)	1.565(-3)	3.100(-3)	3.727(-3)	1.373(-3)	4.888(-4)	2.935(-6)	0.	0.	1.044(-2)
Sum	4.082(-2)	2.969(-1)	2.684(-1)	2.969(-1)	3.017(-1)	3.459(-1)	1.769(-1)	1.186(-1)	1.030(-1)	1.189(-1)	2.068

* Each bin heading gives the upper limit of that bin
* Lower bound of 0.03 column is 0.02 MeV
† Read 4.857(-6) as 4.857×10^{-6}

The differential number flux densities of case D exhibit no large fluctuations in the entire region above 0.06 MeV (that region which should contribute over 90 percent of the total kerma rate), and rejecting this case in its entirety would have the effect of ignoring this large body of apparently useful data. Therefore, it was decided to make adjustments to the poorly behaved low-energy intervals and use the data of case D in the determination of the buildup factor for the air-compressed air geometry.

Since the total scattered kerma rate is of primary importance and differential number flux densities of secondary importance in this study, the adjustments in the low-energy intervals of case D were based on kerma rates rather than on smoothed differential number flux densities. Table VIII shows the kerma rate energy distribution for each of the five cases. The raw data columns list the unadjusted fraction of

the total kerma rate contributed by scattered photons in each of the indicated energy intervals. To adjust the raw data of case D in the three lowest energy intervals, an arbitrary assignment of the highest kerma rate found in the respective bins of any of the other four cases (A, B, C or E) was made for each of these three energy intervals. The highest (rather than average) value was chosen to minimize the effect of this adjusting process which must result in lowering the total kerma rate. The kerma rates in each of the seven higher energy intervals were not altered. The total scattered kerma rate was then recomputed by summing the adjusted contributions over all energy intervals, which for case D was found to be 2.03×10^{-8} ergs g^{-1} sec^{-1}. The resulting adjusted energy fractions are shown in Table VIII and, for comparison, the distribution from the extended air-ground calculations is also listed.

Table VIII. Kerma Rate Energy Distributions

Energy interval (MeV)	Fraction of total kerma rate from scattered photons						
	Raw data					Adjusted values	Extended air-ground calculation
	Case						
	A	B	C	D	E	D	
.02 - .03	.004	<.001	.002	.063	.002	.006	.001
.03 - .04	.006	.008	.007	.230	.007	.012	.003
.04 - .06	.014	.016	.021	.080	.017	.024	.012
.06 - .10	.026	.032	.075	.020	.034	.031	.026
.10 - .18	.057	.085	.066	.046	.070	.071	.068
.18 - .30	.262	.114	.128	.087	.133	.133	.130
.30 - .50	.132	.124	.154	.096	.155	.147	.149
.50 - .75	.109	.103	.137	.105	.253	.160	.129
.75 - 1.00	.161	.205	.197	.092	.140	.141	.135
1.00 - 1.25	.228	.313	.213	.181	.189	.277	.346

As will be seen in the discussion below concerning errors, it was also necessary to adjust the value of the total scattered number flux density for case D. This was accomplished by dividing the adjusted kerma rates in each energy interval by the respective fluence-to-kerma factor to obtain adjusted number flux densities for each, and then summing over all intervals. The value thus determined for the adjusted case D total collided number flux density is 1.38 photons cm^{-2} sec^{-1}.

After these adjustments to case D were made, the average total scattered kerma rate for all five cases was found to be 2.38×10^{-8} ergs g^{-1} sec^{-1} for the normalized source strength of one 1.25 MeV photon emitted isotropically per cm^2 of source area per second. The average total collided number flux density was found to be 1.64 photons cm^{-2} sec^{-1}. The uncollided number flux density at an aboveground air density of 0.001205 g cm^{-3} has been computed analytically to be 2.27 photons cm^{-2} sec^{-1}. Applying to this value Henderson's[14] fluence-to-kerma factor of 5.34×10^{-8} ergs cm^2 g^{-1} for 1.25 MeV photons results in a kerma rate for the uncollided component of 1.21×10^{-7} ergs g^{-1} sec^{-1}. The buildup factor thus becomes

$$1 + \frac{2.38 \times 10^{-8}}{1.21 \times 10^{-7}} = 1.20.$$

Note that if the data from case D were used in their original, unadjusted state, the buildup factor derived from the five cases is 1.21.

As in the extended air-ground calculations, a rigorous computation of the error is impossible, and the best that can be done is to make a judgment from the deviations which were computed by the LO5 procedure. Given the deviations about the scattered flux density for each of the five 11,500-history cases, the deviations about the average value for all 57,500 histories may be computed by straightforward means. However,

before this may be done the deviation of the adjusted flux density of case D must be estimated.

The computed percent deviation in the total number flux density for the unadjusted case D data was an abnormally high 59 percent, caused by the fluctuations in the three low-energy groups. However, the average of the percent deviations in the seven important higher energy intervals of case D was 14 percent and is as low as similar averages for any of the four cases, which were 26, 26, 15 and 14 percent for cases A, B, C and E respectively. It seems reasonable to assume that the percent error in the adjusted total collided flux density of case D would not be greater than that computed by averaging the errors (Table IV) of the other four cases. Thus, while recognizing the lack of rigor in such an approach and without further justification, we have assigned a value of 16 percent as the percent deviation in the adjusted total scattered flux density of case D.

Given the deviation and the total collided flux densities for each of the five cases, the deviation d for all five cases taken together is computed by the relation

$$d^2 = \frac{N_o^2}{N^2} \sum_{j=1}^{5} d_j^2 - \frac{1}{N^2} \left\{ \sum_{j=1}^{5} N_o \bar{\varphi}_j^2 - N \bar{\varphi}^2 \right\}$$

in which

N_o = number of histories per case

N = ΣN_o = total number of histories

d_j = deviation for the jth case (photons cm^{-2} sec^{-1})

$\bar{\varphi}_j$ = total computed number flux density for the jth case, and

$\bar{\varphi}$ = $\frac{1}{5} \sum_{j=1}^{5} \bar{\varphi}_j$.

The second term is a correction making a negligible contribution to the entire expression, and d^2 may be computed simply by evaluating the expression

$$\left[\frac{N_0}{N}\right]^2 \sum_{j=1}^{5} d_j^2$$

For the data listed in Table IV, $d^2 = 0.0169$ and $d = 0.130$ photons cm^{-2} sec^{-1}. Since $\bar{\phi}$ 1.64 photons cm^{-2} sec^{-1}, the percent deviation in the collided number flux density is $\frac{0.130}{1.64} \times 100\% = 8\%$.

In this situation, we have five estimates and an alternative approach to estimating error can be made. The standard error of the mean can be estimated by the relation

$$d^2 = \frac{1}{n(n-1)} \sum_{j=1}^{5} (\bar{\phi}_j - \bar{\phi})^2$$

in which n 5. Evaluating this expression, $d^2 = 0.018$ and $d = 0.134$ photons cm^{-2} sec^{-1}. This value is not significantly different from that computed earlier, and it is reasonable to assume that an error of 8 percent can be associated with the average value of the total collided flux density for all 57,500 histories. Applying the same reasoning as was done in estimating error for the extended air-ground calculations, it can be stated with a fair degree of confidence that the air-compressed air calculation is no more than 10 percent in error in the scattered component of the total kerma rate, and that the buildup factor may be assigned a value of $1.20 \pm .02$.

IV. SUMMARY AND CONCLUSIONS

This study was undertaken to resolve rather large differences in the reported values of the buildup factor 3 feet above a smooth, infinite air-ground interface

uniformly contaminated with ^{60}Co. In particular, experimentally determined values for the buildup factor ranged from 1.15 to 1.38, with the unweighted average value for the four experimental studies quoted in Table I being 1.23. The four moments method values ranged from 1.21 to 1.23 with an average of 1.22, while the four Monte Carlo values ranged from 1.15 to 1.22 with an average of 1.18.

The range of the experimental values can be explained by the difficulty of the measurement and complicating geometry factors such as source asymmetry, source encapsulation, and ground roughness. Although the experimental data are necessary to verify the calculational techniques employed, highest precision in the determination of the buildup factor (e.g., ± 1 percent) has been obtained by calculational means. However, as noted above, differences on the order of 5 percent existed in the various calculated data previously reported.

To examine these differences in the calculated data, four possible explanations were hypothesized:

1. Low-energy photons (< 0.04 MeV), ignored in most Monte Carlo calculations, make a contribution to the total kerma rate which might not be insignificant.

2. The number of histories followed in the earlier Monte Carlo calculations was not sufficient to reduce the statistical uncertainty of the results to a point where the difference between the Monte Carlo and moments results was significant.

3. Compressed air or water does not replicate the photon transport properties of soil, and this factor accounts for the difference between the Monte Carlo studies which use soil and the moments method models which use compressed air or water to represent soil.

4. There is an inherent difference between the Monte Carlo process and the moments method such that the Monte Carlo estimates converge toward a different, lower value than do estimates generated by the moments method.

The first hypothesis was refuted by both the extended air-ground calculations and the air-compressed air calculations. Both sets of computations indicated that photons below 0.06 MeV contribute only about 2 percent to the total scattered kerma rate; the effect of such a contribution on the buildup factor is less than 0.5 percent.

The second hypothesis was supported by both sets of calculations. When the French calculation of 2300 histories was extended to 19,320 histories, a 33 percent increase in the scattered kerma rate was observed. Further, the differences among the five 11,500-history air-compressed air calculations illustrate the fact that far more than 10,000 histories are necessary if one is to obtain highly precise results by applying standard Monte Carlo techniques.

Conclusions about the last two hypotheses cannot be stated with as high a degree of certainty as were the first two, but both the third and fourth hypotheses appear to be in doubt. The extended air-ground Monte Carlo calculation resulted in a buildup factor of $1.21 \pm .02$. The 57,500-history air-compressed air calculation produced a buildup factor of $1.20 \pm .02$, while the NBS moments method result for an identical geometry is quoted as $1.21 \pm .01$. The errors associated with each value are such that the differences in the results cannot be assumed to be real. In fact, one may state with a high degree of confidence that if the effects of hypotheses three or four exist at all (individually or collectively), they can account for no more than a 2 percent difference in the computed buildup factors.

Clearly, both the extended air-ground and the air-compressed air Monte Carlo calculations support the NBS moments method results. Although the Monte Carlo studies reported herein did not attain the 1 percent precision achieved in the NBS moments calculation and one cannot, therefore, assume that the buildup factor for the actual geometry is known with this accuracy, the large differences between previously reported moments method and Monte Carlo results have been resolved to a point where something less than a 2 percent error in the stated value of the buildup factor is very probable. Thus, it is recommended that a value of $1.21 \pm .02$ be assigned to the buildup factor 3 feet above an infinite air-ground interface uniformly contaminated with ^{60}Co.*

* As this report is being published, a new Monte Carlo result was reported. Kalos[16] used an adjoint solution of the transport calculation to compute a buildup factor of 1.196 ± 0.015.

REFERENCES

1. Alberg, M., O'Brien, K. and McLaughlin, J. An experimental determination of differential energy and angle spectra for Cs-137 gamma rays in water. Trans. Am. Nucl. Soc. 9:349, 1966.

2. Batter, J. Cobalt and iridium buildup factors near the ground/air interface. Trans. Am. Nucl. Soc. 6:198, 1963.

3. Beck, H. and Bennett, B. Polynomial solutions of the gamma-ray transport equation in infinite-homogeneous and two-medium plane geometry. Trans. Am. Nucl. Soc. 10:400-401, 1967.

4. Berger, M. J. Calculation of energy dissipation by gamma radiation near the interface between two media. J. Appl. Phys. 28:1502-1508, 1957.

5. Berger, M. J. (personal communication, July 1967).

6. Clarke, E. T. and Buchanan, J. O. Radiation shielding against fallout. Nucleonics 20:143-146, 1962.

7. Collins, D. G. Utilization instructions for general application of the LO5 Monte Carlo procedure. Bethesda, Maryland, Armed Forces Radiobiology Research Institute Contract Report CR65-1, 1965 (originally issued as Radiation Research Associates, Inc. Report RRA-T44, Fort Worth, Texas, 1964).

8. Collins, D. G. and Wells, M. B. COHORT, a Monte Carlo Program for Calculation of Radiation Heating and Transport, Vols. I-IV. Fort Worth, Texas, Radiation Research Associates, Inc. Report RRA-T62, 1966.

9. Davis, F. J. and Reinhardt, P. W. Radiation measurements over simulated plane sources. Health Physics 8:233-243, 1962.

10. French, R. L. Gamma-ray energy and angular distributions above fallout. Health Physics 11:369-383, 1965.

11. French, R. L. (personal communication, June 1967).

12. Garrett, C. W. On the low-energy component of the total dose for deep-gamma penetrations. Trans. Am. Nucl. Soc. 8:648-649, 1965.

13. Goldstein, H. Fundamental Aspects of Reactor Shielding, pp. 172-192. Reading, Massachusetts, Addison-Wesley Publishing Co., 1959.

14. Henderson, B. J. Conversion of neutron or gamma ray flux to absorbed dose rate. Cincinnati, Ohio, General Electric Co. Report XDC 59-8-179, 1959.

15. Kalos, M. H. On the estimation of flux at a point by Monte Carlo. Nucl. Sci. Eng. 16:111-117, 1963.

16. Kalos, M. H. Monte Carlo integration of the adjoint gamma-ray transport equation. Nucl. Sci. Eng. 33:284-290, 1968.

17. Marcum, J. I. Comparison of Monte Carlo calculations with experimental results for the propagation of gamma rays near an air-ground interface. Santa Monica, California, The Rand Corporation Memorandum RM-3399-PR, 1962.

18. Marshall, J. D. and Wells, M. B. The effect of cutoff energy on Monte Carlo calculated gamma-ray dose rates in air. Trans. Am. Nucl. Soc. 9:343-344, 1966.

19. Plummer, G. E. and Miller, W. G. Geometry and barrier attenuation generated by a vertical slab exposed to a plane Co^{60} source. San Francisco, California, U. S. Naval Radiological Defense Laboratory Report USNRDL-TR-677, 1963.

20. Rexroad, R. E. and Schmoke, M. A. Scattered radiation and free-field dose rates from distributed cobalt-60 and cesium-137 sources. Army Chemical Center, Maryland, Nuclear Defense Laboratory Report NDL-TR-2, 1960.

21. Schlemm, C. L., Anthony, A. E., Jr. and Burson, Z. G. Scattered gamma radiation measurements from a Co^{60} contaminated field. Kirtland Air Force Base, New Mexico, Air Force Special Weapons Center Report AFSWC-TN-59-6, 1959.

22. Spencer, L. V. Structure shielding against fallout radiation from nuclear weapons. Washington, D. C., National Bureau of Standards Monograph 42, 1962.

BLANK PAGE

APPENDIX A

Problems inherent in the use of the $\frac{1}{r^2}$ term (r = distance from collision point to receiver point) as a part of the flux density estimator have been discussed by Kalos.[15] Not only is an infinite variance and a preferential tendency to converge from below associated with the total flux density computation, but in computing differential angle and energy distributions, a few "close-in" collisions (collisions occurring very close to the receiver point) produce anomalies in the differential distributions. This derives from the fact that in such cases, $\frac{1}{r^2} >> \left(\frac{1}{r^2}\right)$ where $\left(\frac{1}{r^2}\right)$ is the average value for all collisions, and the differential flux density estimate for these "close-in" collisions becomes large. An example of such behavior which occurred in the extended air-ground calculations is seen in the 160^{o}-170^{o}, 0.3-0.5 MeV angle-energy bin of Table II. As is always the case in the bin associated with a close-in collision, the flux density estimate is high. Although not as obvious, the effect is also displayed in the 90^{o}-100^{o}, 1.0-1.25 MeV bin.

To derive differential distributions from the raw data, it is necessary to smooth the peaks caused by close-in collisions. This may be accomplished by two-dimensional (angle and energy) interpolation, although it must be recognized that actual fine structure can be obliterated in the process. However, when the total flux density or its related quantities, kerma rate and buildup factor, are required, the differential data peaks should not be indiscriminately reduced, since such a process always results in a lower flux density and kerma rate.

The close-in collision difficulty arises because the volume immediately surrounding the receiver point is inadequately sampled for collision points. The

geometry of this situation is shown in Figure A-1. Where only a few close-in collision points are used to sample the volume near the receiver, the large contributions to the flux density from the particles involved in the collisions are deposited in equally few angle-energy bins. Were the volume adequately sampled, contributions of like magnitude would exist in all bins and the anomalies would not exist. In general, for the close-in collisions, the length R_1 (Figure A-1) of the previous flight of the particle is large with respect to the length of the last flight R_2, and the collision point could have been chosen anywhere within the close-in volume with almost equal probability. (One way to handle the problem would be to split the particle whenever $R_2 << R_1$, and force the resulting particles to undergo a collision in each angle bin at a distance R_2 from the receiver, adjusting particle weighting-factors as necessary. However, because of the reprogramming and validation which would be required, this was not done in the calculations reported here.)

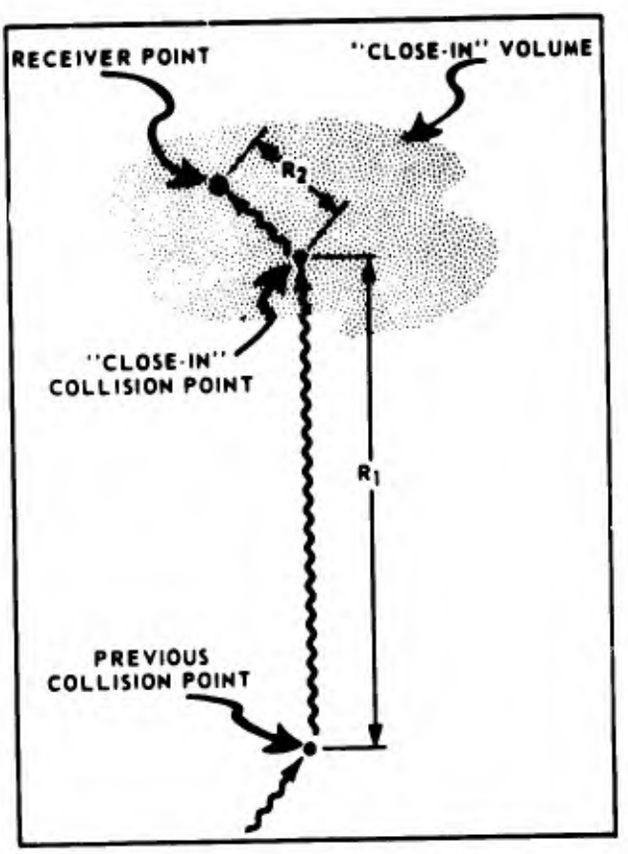

Figure A-1. Close-in collision point geometry

Thus, in the estimate of the integrated flux density, the few close-in collisions must be viewed as a part of the estimate of the contribution from all collision centers near the receiver (albeit from an inadequate sample) and these estimates should not be reduced without sound justification.

UNCLASSIFIED
Security Classification

DOCUMENT CONTROL DATA · R & D

Security classification of title, body of abstract and indexing annotation must be entered when the overall report is classified

1. ORIGINATING ACTIVITY (Corporate author)
Armed Forces Radiobiology Research Institute
Defense Atomic Support Agency
Bethesda, Maryland 20014

2a. REPORT SECURITY CLASSIFICATION
UNCLASSIFIED

2b. GROUP
N/A

3. REPORT TITLE
THE RADIATION ENVIRONMENT ABOVE AN AIR-GROUND INTERFACE COVERED WITH ^{60}Co

4. DESCRIPTIVE NOTES (Type of report and inclusive dates)

5. AUTHOR(S) (First name, middle initial, last name)
C. W. Garrett

6. REPORT DATE	7a. TOTAL NO. OF PAGES	7b. NO. OF REFS
January 1968	34	22

8a. CONTRACT OR GRANT NO	9a. ORIGINATOR'S REPORT NUMBER(S)
b. PROJECT NO	AFRRI SR68-1
c. R MD 4 908	9b. OTHER REPORT NO(S) (Any other numbers that may be assigned this report)
d.	

10. DISTRIBUTION STATEMENT
Distribution of this document is unlimited

11. SUPPLEMENTARY NOTES	12. SPONSORING MILITARY ACTIVITY
	Defense Atomic Support Agency Washington, D. C. 20305

13. ABSTRACT

A review has been made of experimental and theoretical determinations of the buildup factor 3 feet above an infinite air-ground interface uniformly covered with ^{60}Co. Experimental values of the buildup factor range from 1.15 to 1.38 and theoretically calculated values range from 1.15 to 1.23. A new series of Monte Carlo calculations is reported that tests various hypotheses which could account for this range of uncertainty. It is concluded that the substitution of compressed air or water for soil (required in the theoretical method of moments) is valid and that any intrinsic differences between the moments method and Monte Carlo techniques can account for no more than a 2 percent difference in the estimation of the buildup factor. A best value of 1.21 ± .02 may be assigned to the buildup factor 3 feet above an infinite air-ground interface contaminated with ^{60}Co. Angle and energy distributions of the photon number flux density for this geometry are also presented.

DD FORM 1 NOV 65 1473 (PAGE 1)
S/N 0101-807-6801

UNCLASSIFIED
Security Classification

KEY WORDS	LINK A		LINK B		LINK C	
	ROLE	WT	ROLE	WT	ROLE	WT